SSRG International Journal of Thermal Engineering
ISSN: 2395-0250/ https://doi.org/10.14445/23950250/IJTE-V12I2P101

Volume 12 Issue 2, 1-18, May-Aug 2026

Original Article

Artificial Intelligence-Guided Bifurcation Control and Reduced-Order Modeling of Nonlinear Wave Energy Converter Dynamics

Lakshmi. N. Sridhar

Department of Chemical Engineering, University of Puerto Rico, Mayaguez, PR.

Corresponding Author : lakshmin.sridhar@upr.edu

Received: 05 June 2025 Revised: 08 July 2026 Accepted: 25 July 2026 Published: 11 August 2026

Abstract *- This study offers a reduced-order model, bifurcation analysis, and optimal control framework for a nonlinear floating wave-energy converter interacting with an incompressible free-surface fluid. Starting with a potential-flow formulation of wave-structure interaction, a Galerkin projection is used to create a low-dimensional nonlinear dynamical system. This system retains the main hydrodynamic mechanisms, such as resonance effects, radiation damping, nonlinear restoring forces, and modal coupling with secondary hydrodynamic interactions. The resulting model provides a workable representation of a complex fluid-structure system suitable for stability and control analysis. Bifurcation analysis of the reduced system is carried out using numerical continuation. This process reveals a Hopf bifurcation at the trivial equilibrium state. The first Lyapunov coefficient calculated is negative. This confirms a supercritical bifurcation that leads to stable limit-cycle oscillations. These self-sustained oscillations reflect the relevant dynamics between waves and the buoy, resulting from the balance of hydrodynamic forcing, nonlinear damping, and restoring effects. The appearance of bounded periodic solutions shows how nonlinearities help regulate energy transfer and create stable operating conditions for wave-energy conversion. An optimal control formulation is created to maximize energy harvesting through the power take-off mechanism while managing oscillatory behavior. The control input is integrated directly into the nonlinear oscillator dynamics. A soft stability constraint is added to control the system's distance from the Hopf bifurcation boundary. Numerical results indicate that stability-aware control improves performance. This suggests that controlled nonlinear dynamics lead to better energy extraction. The findings demonstrate that bifurcation-informed control strategies can significantly impact wave-energy converter performance. They balance resonance exploitation with nonlinear stability constraints. The proposed framework combines reduced-order modeling, nonlinear dynamical systems theory, and optimal control into a single approach for analyzing and optimizing wave-energy systems in strongly nonlinear conditions.*

Keywords *- Wave Energy Conversion, Nonlinear Dynamics, Hopf Bifurcation, Reduced-Order Modeling, Optimal Control.*

1. Introduction

The growing need for renewable energy has sparked interest in converting ocean wave energy into a dependable resource. Among various technologies, floating point-absorber wave energy converters stand out due to their simple design and ability to harness energy from waves coming from all directions. However, these devices perform according to complex interactions between fluid and structure. These interactions involve changes in the water surface, energy loss due to radiation, resonance effects, and nonlinear restoring forces. Such effects become especially noticeable near resonance, where small changes can significantly alter how the system behaves. This includes the development of persistent oscillations and complex dynamic shifts.

Theoretically, wave-structure interaction in these systems is best explained by combining free-surface potential flow theory with rigid-body dynamics. While this approach is well known, applying it directly in numerical models often leads to complicated and resource-intensive models that are not effective for systematic bifurcation analysis or control-system design. Nonlinear boundary conditions at the water's surface add more challenges, both analytically and numerically. Because of this, there is growing interest in reduced-order modeling strategies that maintain essential hydrodynamic principles while allowing for simpler analyses of nonlinear dynamics, stability limits, and control effectiveness.

Reduced-order models that use modal decomposition effectively capture the main energy structures of the flow. By projecting the governing equations onto carefully chosen spatial eigenfunctions, it is possible to create low-dimensional dynamical systems that keep key features of wave dispersion, nonlinear interactions, and fluid-structure feedback. Near the start of instability, these systems usually depend on a small number of interacting modes, leading to simplified representations of nonlinear oscillators. These reduced models are particularly useful for studying resonance and bifurcation phenomena, including Hopf bifurcations that lead to periodic oscillations.

Alongside advancements in reduced-order modeling, there is an increasing awareness of the significance of optimal control in improving the efficiency of wave-energy systems. The power take-off mechanism is crucial for managing energy flow between the fluid and the structure, and its adjustments can greatly affect both the energy harvested and the system's stability.

Traditional control methods often rely on linear models and struggle to account for nonlinear effects associated with large oscillations and bifurcation-driven dynamics. This limitation drives the need for nonlinear, physics-informed optimal control strategies that account for the system's hydrodynamic structure.

This study tackles these challenges by creating a combined framework for bifurcation analysis, reduced-order modeling, and optimal control of a nonlinear wave-energy converter. Using a free-surface potential flow formulation, a Galerkin projection is applied to develop a low-dimensional nonlinear dynamical system that captures the main wave-buoy interaction mechanisms.

The model shows complex nonlinear behavior, including resonance effects, mode interactions, and Hopf bifurcation-induced limit cycles. This setup allows for an investigation into how nonlinear hydrodynamic effects impact stability and energy extraction performance.

Building on this reduced-order approach, the study incorporates optimal control strategies to maximize energy harvest while managing oscillatory dynamics. The control input, which represents the power take-off force, is integrated directly into the nonlinear oscillator equations. This allows the control action to interact with the system's built-in bifurcation patterns. This interaction enables an examination of how stability requirements and energy-harvesting goals can compete or work together to shape the system's long-term behavior. Particularly, it explores the role of Hopf bifurcations as a key mechanism affecting the shift between stable states and ongoing oscillatory behaviors.

In summary, this study aims to create a cohesive framework for understanding and managing nonlinear wave-energy systems by combining bifurcation theory, reduced-order modeling, and optimal control. By keeping the essential physics of free-surface hydrodynamics while simplifying computational demands, the proposed approach lays the groundwork for a thorough analysis of stability, resonance, and energy harvesting in floating ocean-energy converters.

2. Literature Review

Research on wave energy conversion has changed significantly over the past two decades. It began with basic theoretical and physical studies of how waves interact with structures. Early contributions by Falnes in 2002 established the main principles of oscillating systems for extracting energy from ocean waves. His work provided a solid theoretical basis for understanding resonance, phase control, and optimal energy absorption. This, along with his later review in 2007, highlighted the importance of reactive control and resonance tuning in improving the efficiency of wave energy capture. Around the same time, Evans in 2007 developed classic formulas for wave power absorption by oscillating bodies, which are still fundamental in modern hydrodynamic modeling. These early studies framed wave energy conversion as a problem of fluid-structure interaction, guided by linear potential flow theory and strong resonance characteristics.

Building on these foundations, the 2000s and early 2010s saw many developments in control-oriented frameworks for Wave Energy Converters (WECs). Korde in 2002 introduced early control concepts for wave energy devices, while Babarit and Clément in 2006 looked into optimal control strategies to improve energy capture in both regular and irregular seas. Hals, Falnes, and Moan in 2011 advanced this area by formulating optimal control problems for heaving buoy systems, incorporating hydrodynamic effects and power take-off constraints. These studies showed that optimal control theory could significantly boost energy extraction compared to passive or purely reactive systems, especially when control inputs could actively shape device dynamics.

During this time, there was a move toward computational optimal control frameworks. Abraham and Kerrigan in 2013 applied optimal control and numerical optimization techniques to wave energy systems. Fusco and Ringwood in 2014 developed strong control strategies for WECs under uncertainty. Ringwood, Bacelli, and Fusco in 2015 further solidified energy-maximizing control methods, stressing the importance of real-time implementation and causal constraints. These studies established that wave energy control problems are non-standard optimal control problems characterized by random forcing, nonlinear constraints, and a strong reliance on hydrodynamic memory effects.

A significant advancement came from systematically applying Pontryagin-based optimal control and numerical methods. Zou et al. in 2016 showed that optimal control solutions for WECs often display singular arcs and bang-bang structures. This revealed the non-smooth nature of optimal energy extraction strategies. Bacelli and Ringwood in 2015 extended these concepts to nonlinear systems, demonstrating that nonlinear hydrodynamics can significantly change the structure of optimal control. Mall and Taheri in 2019 tackled the complexity of switching structures in optimal control using regularization methods, spotlighting the computational challenges tied to discontinuous control profiles. More recent studies by Yetkin et al. in 2020 included control cost penalties and actuator constraints, stressing practical implementation and system robustness.

In parallel with control development, the nonlinear dynamics and reduced-order modeling of WECs have attracted more attention. Genest and Ringwood in 2018 created nonlinear time-domain models that account for hydrodynamic memory effects beyond linear theory.

Meanwhile, Maria-Arenas et al. in 2019 reviewed control strategies that emphasize nonlinear and adaptive approaches. These developments showed that real wave energy systems often function in environments where nonlinearities, modal interactions, and resonance-induced instabilities are significant.

Recently, researchers have increasingly focused on new control methods such as extremum-seeking, model predictive control, and stochastic optimization. Parrinello et al. in 2020 demonstrated adaptive extremum-seeking control for maximizing energy in real-time under changing wave conditions. Wang et al. in 2020 examined optimal load control strategies to enhance power output. Ligeikis and Scruggs in 2023 developed stochastic model predictive control frameworks that explicitly consider wave uncertainty and physical constraints. These works indicate a shift toward data-driven and adaptive control strategies for wave energy systems.

Simultaneously, recent advancements in marine dynamics have highlighted the importance of nonlinear stability and bifurcation phenomena in energy conversion systems. Fossen in 2005 pointed out the role of bifurcation theory, showing that transitions like Hopf bifurcations can significantly change system behavior and energy capture efficiency. Similarly, Davidson et al. in 2025 reviewed parametric resonance and nonlinear instability mechanisms in offshore energy systems, underlining the need for unified models that integrate hydrodynamic and structural nonlinearities.

Overall, the literature shows a clear progression from linear resonance-based theory to modern nonlinear, control-oriented, and bifurcation-aware frameworks. Despite significant advancements, a key gap remains in merging reduced-order nonlinear hydrodynamic modeling, bifurcation analysis, and optimal control into a single framework.

This work addresses that gap by combining Galerkin-based model reduction, Hopf bifurcation analysis, and optimal energy-harvesting control, allowing for a systematic investigation of nonlinear wave-structure interactions and their use for better energy conversion.

2.1. The Main Objective of this Research

The main goal of this research is to create a simplified modeling and control system for nonlinear interactions between waves and structures in floating ocean-energy systems. The study centers on a point-absorber wave energy converter interacting with incompressible free-surface fluid. It aims to capture the key hydrodynamic processes that influence energy exchange, nonlinear oscillations, and stability changes. Specifically, the work aims to connect complex fluid dynamics and simpler nonlinear dynamic systems through a Galerkin-based reduction that retains the main wave-buoy interaction modes while preserving the essential physics of the original free-surface problem.

A key aim is to describe the nonlinear stability structure of the fluid-structure system using bifurcation analysis, focusing on Hopf bifurcation phenomena. The study examines the development of self-excited oscillations and limit-cycle behavior as key hydrodynamic parameters vary. This work provides a clear understanding of how resonance, damping, and nonlinear restoring forces lead to the transition from steady states to constant oscillatory motion. By identifying when Hopf bifurcations occur, the research creates a direct connection between hydrodynamic instability mechanisms and the onset of oscillatory patterns relevant for energy harvesting. Another significant goal is to incorporate this bifurcation structure into a control system for energy extraction. The power take-off system is modeled as an active control input, and the strategy is designed to maximize energy output while also regulating nonlinear oscillations to ensure realistic and stable operation. Unlike traditional methods that treat control and stability separately, this work aims to create a single framework where control actions engage directly with the system's nonlinear dynamics and affect its closeness to bifurcation boundaries.

Lastly, the research aims to show that bifurcation-aware reduced-order modeling can provide a computationally efficient and theoretically sound basis for designing wave energy control strategies. By merging modal decomposition, nonlinear dynamic systems analysis, and optimal control theory, the study strives to develop a framework that can predict, regulate, and utilize nonlinear hydrodynamic effects to enhance energy harvesting performance. This integrated approach paves the way for intelligent, physics-based control of ocean-energy systems in highly nonlinear and dynamically complex wave settings. The paper is organized as follows. The model equations are first described, followed by the numerical procedures, results, discussion, and conclusions.

2.2. Novelty of this Work

Although significant progress has been made in modeling and controlling wave energy converters, previous studies have mainly focused on individual aspects rather than developing a cohesive framework. Early research by Falnes (2002, 2007) laid the theoretical groundwork for wave-energy conversion using linear potential-flow theory. Meanwhile, Evans (2007) and Clément et al. (2002) looked at hydrodynamic wave–structure interaction and energy absorption. Later studies by Babarit and Clément (2006), Hals et al. (2011), Abraham and Kerrigan (2013), Ringwood et al. (2015), and Zou et al. (2017) primarily focused on optimal control strategies to maximize power extraction. More recent work by Bacelli and Ringwood (2015), Genest and Ringwood (2018), and Maria-Arenas et al. (2019) included nonlinear hydrodynamic effects and improved control methods. However, these studies generally rely on either detailed numerical models or simpler models that do not directly connect to the bifurcation structure that governs system stability.

The main innovation of this work is the integration of consistent reduced-order modeling with nonlinear bifurcation analysis, optimal control, and artificial intelligence within a single computational framework. Beginning with the governing free-surface potential-flow equations, a Galerkin projection is used to derive a nonlinear reduced-order model that captures the key wave–structure interaction mechanisms. Unlike earlier studies, this reduced model is designed to identify Hopf bifurcations and nonlinear limit-cycle oscillations. This allows for a systematic analysis of the stability boundaries of the wave-energy converter using continuation methods.

Another advancement is the addition of Hopf-bifurcation-aware optimal control. Instead of maximizing harvested power without considering nonlinear dynamics, this formulation takes into account how close the operating point is to oscillatory instability through a soft stability penalty. This helps the controller maximize energy extraction while avoiding unwanted limit-cycle behavior. The framework establishes a direct link between nonlinear dynamical systems theory and wave-energy optimization, a topic that has received little attention in existing research.

Finally, this work presents an artificial intelligence-assisted reduced-order modeling framework that sets the stage for future data-driven stability prediction and real-time control. By merging fundamental hydrodynamic modeling with reduced-order nonlinear dynamics, bifurcation theory, artificial intelligence, and optimal control, this proposed method offers a unified and efficient approach for analyzing and intelligently controlling nonlinear ocean wave-energy systems. This integration of various fields marks a significant improvement over earlier studies, which often viewed reduced-order modeling, bifurcation analysis, artificial intelligence, and optimal control as distinct challenges rather than parts of a unified physics-informed framework.

2.3. Model Equations

The ocean-energy system considered in this work consists of a floating point-absorber wave energy converter interacting with an incompressible free-surface fluid domain. The system is intended to model nonlinear wave–structure interactions in ocean-wave energy-harvesting devices and to provide a fluid-mechanically consistent framework for bifurcation analysis, artificial-intelligence-assisted reduced-order modeling, and optimal control design. The physical configuration consists of a floating buoy partially submerged in water and subjected to incident surface waves. The buoy's oscillatory motion is coupled to the surrounding fluid through hydrodynamic pressure and free-surface deformation.

The fluid is assumed to be incompressible and irrotational. Under these assumptions, the velocity field may be represented through a scalar velocity potential. Let $\phi(x, y, t)$ denote the velocity potential of the fluid, where $x$and $y$are the horizontal coordinates, $z$is the vertical coordinate, and $t$represents time. The fluid velocity vector is therefore given by $\mathbf{u} = \nabla\phi$ where $\mathbf{u}$ denotes the fluid velocity field. Since the fluid is incompressible, conservation of mass requires that the velocity potential satisfy Laplace's equation throughout the fluid domain.

$$\nabla^2\phi = \left(\frac{\partial^2\phi}{\partial x^2}\right) + \left(\frac{\partial^2\phi}{\partial y^2}\right) + \left(\frac{\partial^2\phi}{\partial z^2}\right) = 0 \tag{1}$$

The free surface of the ocean is represented by

$$z = \eta(x, y, t) \tag{2}$$

where $\eta(x, y, t)$ denotes the free-surface elevation relative to the mean water level. At the free surface, both kinematic and dynamic boundary conditions must be satisfied.

The kinematic boundary condition ensures that fluid particles located on the free surface remain on the free surface during the evolution of the flow. This condition is written as

$$\frac{\partial\phi}{\partial z} = \frac{\partial\eta}{\partial t} + \frac{\partial\phi}{\partial x}\frac{\partial\eta}{\partial x} + \frac{\partial\phi}{\partial y}\frac{\partial\eta}{\partial y} \tag{3}$$

evaluated at the free surface $z = \eta(x, y, t)$.

The dynamic boundary condition follows from Bernoulli's equation and relates the pressure and fluid motion at the free surface. Assuming atmospheric pressure at the interface, the dynamic boundary condition becomes

$$\frac{\partial\phi}{\partial t} + \frac{1}{2}|\nabla\phi|^2 + g\eta + \frac{p}{\rho} = 0 \tag{4}$$

where g denotes the gravitational acceleration, $p$is the pressure field, and ρ is the fluid density. This equation is also evaluated at the free surface.

The ocean bottom is assumed to be rigid and impermeable. If the undisturbed water depth is denoted by h, the bottom boundary is located at ($z= -h$), and the no-penetration condition at the bottom requires $\left(\frac{\partial\phi}{\partial z} = 0\right)$ at $z = -h$.

The floating buoy undergoes vertical oscillatory motion under the action of hydrodynamic wave forcing. Let $\eta_b(t)$ denote the vertical displacement of the buoy from its equilibrium position. The buoy dynamics are governed by Newton's second law. Including hydrodynamic added mass, radiation damping, hydrostatic restoring forces, and nonlinear hydrodynamic contributions, the governing equation for the buoy motion may be expressed as

$$m\frac{\partial^2\eta_b}{\partial t^2} + c_{PTO}\frac{\partial\eta_b}{\partial t} + k_h\eta_b = F_h \quad (5)$$

where m denotes the physical mass of the buoy, $c_{PTO}$is the damping coefficient associated with the power take-off system, $k_h$is the hydrostatic restoring stiffness, and $F_h$represents the net hydrodynamic force exerted by the fluid.

The hydrodynamic force contains several contributions associated with incident wave forcing, radiation damping, added mass effects, and nonlinear wave–structure interactions. A simplified representation of the hydrodynamic force is given by

$$F_h = F_w - \mu_r\frac{\partial\eta_b}{\partial t} - m_a\frac{\partial^2\eta_b}{\partial t^2} + F_{nl} \quad (6)$$

where $F_w$denotes the excitation force generated by incoming surface waves, $\mu_r$represents the radiation damping coefficient, $m_a$is the hydrodynamic added mass, and F_{nl}denotes nonlinear hydrodynamic effects.

To capture nonlinear oscillatory behavior and the emergence of hydrodynamic instabilities, the model retains weak nonlinearities. The nonlinear hydrodynamic force is approximated using cubic restoring and nonlinear damping terms of the form.

$$F_{nl} = -\alpha\eta_b^3 + \beta\eta_b^2\frac{\partial^2\eta_b}{\partial t^2} \quad (7)$$

where α is the coefficient associated with nonlinear restoring stiffness and βdenotes the nonlinear damping coefficient arising from viscous dissipation and nonlinear wave–body interactions. Substituting the hydrodynamic force expression into the buoy dynamics equation yields the nonlinear wave-energy converter model.

$$(m+m_a)\frac{\partial^2\eta_b}{\partial t^2} + (c_r - u)\frac{\partial\eta_b}{\partial t} + k_h\eta_b + \alpha\eta_b^3 - \beta\eta_b^2\frac{\partial\eta_b}{\partial t} = F_w \quad (8)$$

where $c_r$denotes the effective radiation damping coefficient, and $u(t)$represents the active control input associated with the power take-off mechanism. The control input may correspond to adaptive damping, reactive control, or artificial-intelligence-assisted feedback strategies designed to maximize energy extraction or stabilize nonlinear oscillatory states. Tables 1 and 2 show the parameter and variable details for the PDE.

The coupled free-surface fluid equations together with the nonlinear buoy dynamics constitute a fluid-mechanically consistent PDE–ODE system for the investigation of nonlinear ocean-energy dynamics. The coupled hydrodynamic system admits resonant interactions, self-excited oscillatory states, and nonlinear limit-cycle dynamics arising from Hopf bifurcations. The resulting formulation provides a reduced yet fluid-mechanically consistent framework for the analysis of nonlinear hydrodynamic stability, bifurcation structure, and control-oriented wave-energy dynamics.

The principal variables appearing in the model are summarized as follows. The quantity $\phi(x,y,z,t)$denotes the fluid velocity potential, $\eta(x,y,t)$represents the free-surface elevation, and $\eta_b(t)$corresponds to the vertical buoy displacement. The variable $p$denotes the fluid pressure, while u represents the fluid velocity field. The forcing term $F_w$denotes the hydrodynamic excitation generated by incident surface waves and corresponds to the incident wave forcing, while $u(t)$denotes the control input applied through the power take-off system.

The principal parameters include the buoy mass m, added mass. m_a, radiation damping coefficient c_r, hydrostatic restoring coefficient k_h, nonlinear stiffness coefficient α, nonlinear damping coefficient β, fluid density ρ, gravitational acceleration g, and water depth h. Collectively, these parameters determine the system's nonlinear hydrodynamic response, including resonance behavior, oscillatory stability boundaries, and the onset of Hopf bifurcation dynamics.

To derive a reduced-order nonlinear dynamical system suitable for bifurcation analysis and optimal control, a Galerkin modal decomposition is applied to the coupled free-surface hydrodynamic equations. The objective of the reduction is to retain the dominant nonlinear wave–structure interaction mechanisms while obtaining a tractable low-dimensional representation capable of capturing resonance phenomena, self-excited oscillations, and Hopf bifurcation dynamics.

Since the principal hydrodynamic behavior is governed by a small number of energetic modes near instability onset, the free-surface elevation and velocity potential may be expanded in terms of spatial basis functions satisfying the governing boundary conditions.

The free-surface elevation is represented as

$$\eta(x,t) = \sum_1^N a_n(t)\Phi_n(x) \quad (9)$$

where $a_n(t)$denotes the time-dependent modal amplitudes and $\Phi_n(x)$represents the spatial eigenfunctions associated with the free-surface wave motion. Similarly, the velocity potential is expanded as

$$\phi(x,t) = \sum_1^N b_n(t)\Psi_n(x) \quad (10)$$

where $b_n(t)$denotes the modal coefficients associated with the velocity field and $\Psi_n(x,z)$are hydrodynamic eigenfunctions satisfying Laplace's equation and the corresponding boundary conditions. Near the onset of hydrodynamic instability, the dominant system behavior is typically governed by a finite number of interacting modes. Accordingly, a three-mode truncation is adopted in order to capture the leading-order nonlinear wave–structure interactions. The free-surface elevation, therefore, becomes

$$\eta(x,t) = a_1(t)\Phi_1(x) + a_2(t)\Phi_2(x) + a_3(t)\Phi_3(x) \quad (11)$$

while the velocity potential is approximated by

$$\phi(x,t) = b_1(t)\Psi_1(x) + b_2(t)\Psi_2(x) + b_3(t)\Psi_3(x) \quad (12)$$

The modal expansions are substituted into the governing fluid equations and free-surface boundary conditions. The Galerkin procedure is then performed by projecting the resulting residual equations onto the retained basis functions.

Defining

$$R_\eta = \frac{\partial \eta}{\partial t} + \nabla\phi.\nabla\eta - \frac{\partial \phi}{\partial z}$$

$$R_\phi = \frac{\partial\phi}{\partial t} + \frac{1}{2}|\nabla\phi|^2 - \frac{\partial\phi}{\partial z} + g\eta \quad (13)$$

We enforce

$$\int_\Omega R_\eta \Phi_i d\Omega = \int_\Omega R_\phi \Phi_i d\Omega = 0$$

These are the Galerkin orthogonality conditions. After enforcing the Galerkin orthogonality conditions, the residual fields $R_\eta$and $R_\phi$are replaced by their projections onto the retained basis functions. Substituting the modal expansions for $\eta$and ϕinto the governing free-surface and Laplace equations and carrying out these projections eliminates all spatial dependence. As a result, all integrals of the form $\int \Phi_i \Phi_j d\Omega$, $\int \Psi_i \Psi_j d\Omega$ and higher-order nonlinear combinations reduce to constant coupling coefficients determined entirely by the chosen eigenfunctions and the geometry of the fluid domain.

The outcome of this projection is a set of coupled ordinary differential equations governing the temporal evolution of the modal amplitudes. $a_i(t)$. These equations take the general nonlinear form

$$\frac{da_i}{dt} = \sum_j L_{ij}a_j + \sum_{j,k} N_{ijk}a_j\, a_k + \sum_{j,k,l} Q_{ijkl}a_j\, a_k a_l \quad (15)$$

where L_{ij}represents the linear hydrodynamic operator arising from wave dispersion, gravity restoring effects, and radiation damping, while N_{ijk} and Q_{ijkl} originate from quadratic and cubic nonlinearities in the free-surface boundary conditions and buoy–fluid coupling terms. The coefficients $L_{ij}, N_{ijk}, Q_{ijkl}$ are explicit integrals of the eigenfunctions and encode all geometric and hydrodynamic information of the original PDE system. The linear, quadratic, and cubic coefficients are

$$L_{ij} = \int_\Omega \quad \Phi_i \frac{\partial R_\eta}{\partial a_j} + \Psi_i \frac{\partial R_\phi}{\partial a_j} d\Omega$$

$$N_{ijk} = \int_\Omega \quad \Phi_i \frac{\partial^2 R_\eta}{\partial a_j \partial a_k} + \Psi_i \frac{\partial^2 R_\phi}{\partial a_j \partial a_k} d\Omega$$

$$Q_{ijkl} = \int_\Omega \quad \Phi_i \frac{\partial^3 R_\eta}{\partial a_j \partial a_k \partial a_l} + \Psi_i \frac{\partial^3 R_\phi}{\partial a_j \partial a_k \partial a_l} d\Omega \quad (16)$$

To obtain a minimal dynamical representation capturing the dominant oscillatory physics, the system is truncated to the leading energetic modes. The first mode is associated with the principal wave–buoy interaction, while the third mode represents the most significant secondary hydrodynamic correction responsible for radiation and free-surface coupling effects. A nonlinear coordinate transformation is then introduced to recast the modal dynamics into a canonical oscillator form. The dominant oscillatory variable is defined as

$$x = a_1(t)$$

$$y = \frac{da_1}{dt} = \frac{dx}{dt}$$

$$z = a_3(t) \quad (17)$$

This transformation isolates the primary oscillatory degree of freedom and separates inertial dynamics from higher-order fluid memory effects. The variable $x(t)$therefore represents the principal wave–buoy oscillation, $y(t)$represents its conjugate momentum or velocity, and $z(t)$captures residual hydrodynamic coupling induced by free-surface deformation and radiation effects that cannot be eliminated through a single-mode reduction.

Expressed in these variables, and retaining only leading-order nonlinear interactions responsible for energy transfer, saturation, and instability onset, the reduced system takes the canonical form of a coupled nonlinear oscillator with hydrodynamic memory:

$$\frac{dx}{dt} = y$$

$$\frac{dy}{dt} = \mu y - \omega^2 x - \alpha x^3 - \beta x^2 y + \gamma z + q(t)$$

$$\frac{dz}{dt} = -\lambda z + \delta x^2 - \sigma xy \qquad (18)$$

where $x(t)$represents the dominant oscillatory wave–buoy displacement mode, $y(t)$corresponds to the modal velocity, and $z(t)$denotes a secondary nonlinear hydrodynamic interaction mode associated with free-surface coupling effects. The quantity $q(t)$represents the control input associated with the power take-off mechanism and may later be determined through optimal control or artificial-intelligence-assisted feedback strategies. Tables 3 and 4 show the parameter and variable details for the reduced ODE.

The analytical expressions for the parameters are

$$\omega^2 \sim \int_\Omega \Phi_1(g\Phi_1 + \nabla\Phi_1.\nabla\Phi_1)d\Omega\,;\ \mu \sim \int_\Omega \Phi_1(\frac{d\Phi_1}{dt})d\Omega\,;$$

$$\alpha \sim \int_\Omega (\Phi_1^3 + \eta_b\Phi_1^2)d\Omega;\ \beta \sim \int_\Omega \Phi_1(\Phi_1^2(\frac{d\Phi_1}{dt}) + \nabla\Phi_1.\nabla(\frac{d\Phi_1}{dt}))d\Omega;$$

$$\gamma \sim \int_\Omega \Phi_1(\frac{d\Psi_3}{dt}) + g\Psi_3)d\Omega + \int_\Omega \Phi_1\nabla\Phi_1.\nabla\Psi_3)d\Omega\,;$$

$$\lambda = \int_\Omega \Psi_3(\frac{d\Psi_3}{dt}) + \nabla\Psi_3.\nabla\Psi_3)d\Omega\ \delta = \sim \int_\Omega \Psi_3(\Phi_1^2 + \nabla\Phi_1.\nabla\Phi_1)d\Omega\,;$$

$$\sigma \sim \int_\Omega \Psi_3\left(\Phi_1\left(\frac{d\Phi_1}{dt}\right) + \nabla\Phi_1.\nabla\left(\frac{d\Phi_1}{dt}\right)\right)d\Omega;\ q(t)\mu \sim \int_\Omega \Phi_1 u(t)d\Omega. \qquad (19)$$

Derivations of these parameters are presented in an appendix. The parameter ω denotes the characteristic wave frequency, while μgoverns the effective hydrodynamic damping of the oscillatory mode—the cubic nonlinear coefficient αrepresents nonlinear restoring effects generated by buoyancy and free-surface deformation. The coefficient βcorresponds to nonlinear damping effects arising from wave radiation and viscous hydrodynamic interactions. The parameter γdetermines the coupling strength between the primary oscillatory mode and the secondary hydrodynamic interaction mode z, whereas λcharacterizes the decay rate of the secondary mode. The nonlinear term δx^2originates from quadratic free-surface interactions generated through the projection of the nonlinear Bernoulli boundary condition onto the retained Galerkin modes. Similarly, the mixed nonlinear interaction term $-\sigma xy$ represents nonlinear modal energy transfer between the oscillatory and hydrodynamic interaction modes. These nonlinear interactions are responsible for amplitude saturation and the emergence of stable or unstable oscillatory states near instability onset. The reduced dynamical system constitutes a nonlinear hydrodynamic oscillator with coupled modal interactions capable of exhibiting resonance phenomena, self-excited oscillations, and nonlinear limit-cycle dynamics. The equilibrium state of the system is obtained by imposing

$$\frac{dx}{dt} = \frac{dy}{dt} = \frac{dz}{dt} = 0 \qquad (20)$$

Linearization about the equilibrium reveals that the system admits oscillatory instability when the effective hydrodynamic damping parameter μcrosses a critical threshold. Under these conditions, a pair of complex-conjugate eigenvalues may traverse the imaginary axis, leading to a Hopf bifurcation and the subsequent emergence of nonlinear periodic oscillations. The principal instability dynamics are governed by the nonlinear oscillatory equation.

$$\frac{dy}{dt} = \mu y - \omega^2 x - \alpha x^3 - \beta x^2 y + \gamma z + q(t) \qquad (21)$$

which combines linear resonance, nonlinear hydrodynamic restoring forces, nonlinear damping, modal interaction effects, and active control forcing within a unified reduced-order framework. The resulting three-dimensional Galerkin model preserves the essential nonlinear hydrodynamic physics of the ocean-energy system while remaining computationally tractable for continuation analysis, bifurcation tracking, optimal control design, and artificial-intelligence-assisted reduced-order modeling of nonlinear wave-energy dynamics.

Here, the coefficient ωrepresents the natural wave–buoy oscillation frequency inherited from the linearized dispersion relation, while μdenotes the effective hydrodynamic damping resulting from the balance between radiation losses and energy input through wave forcing. The nonlinear coefficient αarises from cubic restoring effects associated with finite-amplitude free-surface deformation and buoyancy nonlinearity, whereas βrepresents nonlinear damping contributions due to convective hydrodynamic interactions. The coupling parameter γdescribes energy exchange between the dominant oscillatory mode and the secondary hydrodynamic mode $z(t)$, while λgoverns the decay of this secondary mode and represents the relaxation of hydrodynamic memory. The terms δx^2Moreover, σxyoriginate from quadratic nonlinear interactions in the free-surface boundary conditions and represent mode coupling between elevation and velocity fields.

The term $q(t)$enters through the power take-off mechanism and represents external actuation applied to the buoy system. This term can be interpreted as either passive damping modulation or active feedback control, depending on the design of the energy extraction strategy. Importantly, the presence of $q(t)$does not alter the intrinsic hydrodynamic structure of the system but provides a mechanism for influencing stability boundaries, shifting Hopf bifurcation points, and modifying limit-cycle amplitudes. The resulting three-dimensional system is a minimal nonlinear hydrodynamic oscillator that preserves the essential physics of wave–structure interaction, including resonance, nonlinear saturation, and hydrodynamic coupling effects. It provides a mathematically consistent reduced-order representation of the original free-surface PDE system and serves as a foundation for subsequent bifurcation analysis, optimal control formulation, and data-driven approaches.

2.4. Justification of the Three-Mode Galerkin Reduction

The equations that describe the interaction between the free-surface flow and the floating wave-energy converter are part of a complex fluid-structure interaction problem. After applying the Galerkin method for spatial discretization, the resulting system consists of many coupled nonlinear ordinary differential equations. These equations represent how modal amplitudes change over time. While keeping more modes usually improves the representation of the full hydrodynamic system, it also significantly raises the complexity of bifurcation analysis, continuation calculations, and optimal control. Therefore, it is necessary to create a reduced-order model that maintains the major physical processes while remaining small enough for thorough nonlinear analysis. This work uses a three-mode Galerkin truncation because, near the start of oscillatory instability, the system dynamics are mainly influenced by a few key modes. The first mode captures the main wave-buoy oscillation and contains most of the hydrodynamic energy linked to the incoming wave field. This mode sets the primary resonance behavior of the floating structure, which drives the main energy-harvesting dynamics. The second mode naturally acts as the conjugate velocity variable of the primary oscillatory mode. This changes the governing second-order oscillator equation into a first-order dynamic system that is appropriate for continuation and stability analysis. The third mode addresses the leading corrections due to radiation effects, free-surface memory, and nonlinear interactions that a single oscillator cannot fully describe. By keeping this third mode, the reduced-order model can accurately reflect the essential nonlinear coupling that causes amplitude saturation and self-excited oscillations. Choosing three dynamic variables is also supported by nonlinear bifurcation theory. A two-dimensional autonomous dynamic system cannot capture both modal memory effects and the nonlinear interactions needed to match the observed hydrodynamic behavior. Adding a third state variable gives the necessary dimensionality to represent the link between the primary oscillatory motion and the slower hydrodynamic relaxation processes from wave radiation and free-surface deformation. This interaction leads to Hopf bifurcations and the development of nonlinear limit-cycle oscillations seen in the numerical results. From a physical standpoint, higher-order Galerkin modes relate to smaller spatial scales and hold much less energy than the leading modes during normal operation. Their main role is to introduce refinements to the nonlinear coefficients without significantly changing the behavior near the first instability boundary. Therefore, ignoring these higher modes does not affect the existence of equilibrium solutions, the position of the primary Hopf bifurcation, or the overall structure of the stable limit cycles. Instead, the omitted modes primarily impact details like oscillation amplitudes and higher-frequency harmonics, which become more significant only far from the bifurcation point.

The three-mode approximation thus strikes a good balance between physical accuracy and computational efficiency. It retains the key mechanisms that influence resonance, nonlinear restoring effects, radiation damping, hydrodynamic memory, and modal coupling while creating a compact dynamical system suitable for numerical continuation, stability analysis, and optimal control. The resulting reduced-order model keeps the critical nonlinear physics needed to predict Hopf bifurcations and limit-cycle oscillations while being cost-effective for ongoing optimization and bifurcation studies.

2.5. Bifurcation Analysis and Optimal Control

2.5.1. Bifurcation Analysis

Continuation and bifurcation computations were carried out using the MATLAB-based software MATCONT. Bifurcation analysis provides important insights into the mechanisms underlying the existence of multiple steady states and self-sustained oscillations in nonlinear dynamical systems. In particular, branch points and limit points are associated with the emergence of multiple steady-state solutions, whereas oscillatory dynamics and periodic solutions originate from Hopf bifurcations. The package, originally developed and subsequently enhanced by several researchers, enables the systematic identification of Limit Points (LP), Branch Points (BP), and Hopf Bifurcation Points (H) in nonlinear dynamical models[Dhooge et al (2003). This program identifies Limit Points(LP), Branch Points(BP), and Hopf bifurcation points(H) for a system of ordinary differential equations

$$\frac{dx}{dt} = f(x,\alpha) \qquad (22)$$

$x \in R^n$ where the bifurcation parameter is α , more details can be found in Kuznetsov(1998) and Govaerts(2000).

2.5.2. Optimal Control

Pyomo.dae is used for the Optimal Control calculations in Pyomo.DAE, the continuous-time dynamic model, is transformed into a Nonlinear Programming (NLP) problem through discretization techniques such as orthogonal collocation, allowing the resulting optimization problem to be solved using standard NLP solvers. The NLP is solved using IPOPT (Wachter et al 2006).

2.6. Formation of Stability Dataset from MATCONT Results

A stability dataset was developed from numerical continuation calculations performed in MATCONT. The stability dataset consists of rows, each representing a continuation point from an equilibrium branch. Each row contains the state variables, the bifurcation parameter, and a stability measure. The stability measure is a numerical value derived from the Jacobian matrix. The Jacobian matrix is computed numerically at each equilibrium point. The eigenvalues are then computed automatically using MATLAB. The maximum value of the real part of these eigenvalues is then computed as a scalar stability measure.

The stability measure is computed using "eig_real_max = max(real(eigvals));" in MATLAB. The stability measure is a quantitative metric in which negative values indicate locally asymptotically stable equilibria, positive values indicate instability, and a zero crossing indicates a Hopf bifurcation. The stability dataset is then saved as a CSV file. The dataset can then be used in subsequent computational calculations to perform classification or regression to identify stability boundaries or approximate bifurcations.

2.7. Neural Network Surrogate for Stability Prediction

Direct embedding of eigenvalue calculations into IPOPT-based optimal control is impractical for several reasons: (i) computing eigenvalues at each time step is computationally expensive, (ii) the mapping from states to the maximum eigenvalue is non-smooth near eigenvalue crossings, and (iii) symbolic differentiation of eigenvalues is challenging.

Prior to neural network training, all input variables were standardized to improve numerical conditioning and training stability. Let x_{raw} denote the vector of state variables and bifurcation parameter obtained from the stability dataset. For each input variable j, the training mean $\mu_j$and training standard deviation $\sigma_j$were computed over the training dataset as the arithmetic mean and standard deviation, respectively. The training mean for the input variable j is defined as the arithmetic average over all training samples, $\mu_j = \frac{1}{N}\sum_{k=1}^{N} x_j^{(k)}$ and the training standard deviation for the input variable $j$is defined as: $\sigma_j = \frac{1}{N}(\sum_{k=1}^{N} x_j^{(k)} - \mu_j)^2$

The standardized inputs were defined as

$$x_j = \frac{x_{raw,j} - \mu_j}{max(\sigma_j, \varepsilon_{scale})} \quad (23)$$

where $\mu_j$and $\sigma_j$denote the mean and standard deviation of the j-th training variable, respectively, and $\varepsilon_{\text{scale}}$ is a small positive regularization parameter introduced to prevent numerical singularities associated with extremely small variances in the training dataset. This transformation ensures that each input variable remains properly scaled while avoiding excessively large neural-network activation arguments during optimization. The normalization procedure improves neural-network conditioning and substantially enhances the robustness of gradient-based optimization. The vectors $\mu$and σcomputed during training were stored and embedded identically within the Pyomo optimal-control formulation to ensure consistency between neural-network training and deployment.

To overcome these limitations, a feedforward neural network is trained to approximate the maximum eigenvalue as a smooth function of the system state and bifurcation parameter. A typical architecture employs the hyperbolic tangent (tanh) as a smooth activation function. If the input vector is denoted by x, which represents the scaled variables, then the network is defined as:

The vectors μ, σ $\mu$and σ computed during training were stored and embedded identically within the Pyomo optimal control formulation to ensure consistency between neural network training and deployment.

To overcome these limitations, a feedforward neural network is trained to approximate the maximum eigenvalue as a smooth function of the system state and bifurcation parameter. A typical architecture employs the hyperbolic tangent (tanh) as a smooth activation function. If the input vector is denoted by x, which are the scaled variables, then the network is defined as:

$$\begin{aligned} z1 &= tanh(W1\, x + b1) \\ z2 &= tanh(W2\, z1 + b2) \\ \lambda\_max\_NN &= W3\, z2 + b3 \end{aligned} \quad (24)$$

Because tanh is infinitely differentiable, the network is fully smooth, guaranteeing the availability of first and second derivatives required by IPOPT. Here, W1, W2, and W3 are the weights that scale and combine inputs or hidden-layer features, while b1, b2, and b3 are the biases that allow the neurons to shift their activation independently of the inputs. Without biases, the network output would be constrained to pass through the origin, limiting flexibility.

The hidden-layer outputs z1 and z2 represent nonlinear combinations of the inputs and previous-layer features, respectively. Each element of $z_1$is a smoothed combination of the original inputs, while each element of z2 encodes more abstract patterns extracted from z1.

The final output λ_max_NN provides a smooth approximation of the maximum real eigenvalue, enabling efficient and differentiable stability evaluation within the optimal control problem. The integration into optimal control is done using a soft penalty formulation where we use a smooth_max function that converts λ into a smooth, nonnegative penalty that only "activates" when the system is unstable:

$$s1\,max(_1 \frac{(\lambda+\varepsilon_1)+\sqrt{(\lambda+\varepsilon_1)^2+\varepsilon_1}}{2}_{max} \tag{25}$$

λ is the neural network's predicted maximum eigenvalue at the current state and parameter, while ε is a small positive safety margin to ensure differentiability. The soft penalty formulation involves the new objective function, where the original objective function $optv(t) = (\sum(u(t)y(t))^2 - 0.1(u(t))^2)$ is modified to $\sum(optv(t) + \alpha_{hopf}.s1^2{}_{max}$ α_{Hopf} control how aggressively instability is penalized, and ε_1 prevents numerical issues at exactly λ = 0 and slightly shifts the stability boundary. The goal is to maximize the power harvested by the power take-off system from the oscillatory wave–buoy motion while limiting excessive control effort. The first term represents the energy extracted from the buoy velocity through the control action, whereas the second term penalizes large control inputs in order to maintain physically realistic and stable operation of the wave-energy converter. This ensures differentiability for IPOPT and avoids non-smooth optimization. This approach avoids repeated eigenvalue computations and provides a smooth, differentiable surrogate suitable for gradient-based optimization. Furthermore, this enables the incorporation of stability constraints into optimal control without explicitly computing eigenvalues during optimization.

To facilitate integration into optimal control, a stability dataset is constructed from MATCONT continuation results. At each equilibrium point, the Jacobian is evaluated and its eigenvalues computed. The stability metric is defined as the maximum real part of the eigenvalues ($\lambda_{\max} = \max \Re(\lambda(J))$). Negative values indicate stability, positive values indicate instability, and zero crossings correspond to Hopf bifurcations.

To avoid repeated eigenvalue computations within optimization, a feedforward neural network is trained to approximate the spectral abscissa as a smooth function of the system state and bifurcation parameter. Using hyperbolic tangent activation functions ensures smooth differentiability required by gradient-based solvers. The resulting surrogate provides a differentiable stability indicator suitable for embedding within optimal control formulations.

3. Results

For the bifurcation analysis, μ was selected as the primary continuation parameter. The remaining model parameters were fixed at μ was chosen as the bifurcation parameter, and the values of the other parameters are $(\omega = 1, \alpha = 1, \beta = 0.5, \gamma = 0.8, \delta 0.5, \sigma = 0.3)$. Numerical continuation of the equilibrium solutions was performed using MATCONT. A Hopf bifurcation point was detected at the trivial solution value of [X; Y; Z;μ] values of (0;0;0;0) with a first Lyapunov coefficient value of -2.248401e-01. The limit cycle produced by this Hopf bifurcation is shown in Figure 1a. Computation of the first Lyapunov coefficient yields $l_1 = -2.248401 \times 10^{-1} < 0$, confirming that the Hopf bifurcation is supercritical. Consequently, the loss of stability of the trivial equilibrium gives rise to a stable nonlinear limit cycle corresponding to self-sustained wave–buoy oscillations.

For the optimal control, (μ was selected as the control parameter), when no measures are taken ($\alpha_{hopf} = 0$), $(\sum optv(t))^2$is maximized, and when the soft penalty formulation is integrated, $\sum(optv(t) + \alpha_{hopf}.s1^2{}_{max}$is maximized. When no measures were taken, the obtained value ($\sum optv(t)$) was 3.454. When the soft penalty formulation is integrated, $\alpha_{hopf} = 1$; the obtained value ($\sum optv(t)$) is 3.79. The increase in the objective value when the Hopf constraint is implemented demonstrates that one is able to obtain more energy when the Hopf bifurcations and limit cycles are avoided.

Figures 2a–2b illustrate the optimal control profiles without Hopf bifurcation constraints, while Figures 2c–2d show the corresponding profiles with the stability penalty included.

3.1. Discussion of Results

The bifurcation analysis shows that the reduced-order hydrodynamic oscillator captures the key nonlinear dynamics linked to wave-structure interaction in floating ocean-energy systems. Continuing the equilibrium branch reveals a Hopf bifurcation at the trivial equilibrium state, indicating a shift from a stable stationary setup to self-sustained nonlinear oscillations. The computed first Lyapunov coefficient is negative, confirming that the bifurcation is supercritical. As a result, destabilizing the equilibrium creates a stable limit cycle instead of unstable divergent oscillations. This finding is important because the nonlinear hydrodynamic interactions in the reduced-order model naturally limit oscillation growth due to nonlinear damping and cubic restoring forces. Thus, the resulting bounded periodic response reflects realistic wave-buoy oscillations that can last over long time periods without unlimited amplitude growth. The limit cycle shown in Figure 1a illustrates the onset of sustained nonlinear oscillatory motion after instability begins.

The closed orbit in phase space reflects the balance among wave-induced energy input, hydrodynamic damping, and nonlinear restoring forces related to free-surface deformation and buoyancy effects. The emergence of stable periodic oscillations aligns with classical nonlinear resonance phenomena seen in wave-structure interaction systems. In this model, the cubic nonlinear stiffness and nonlinear damping terms control the oscillation amplitude and prevent runaway resonance growth. The reduced-order system, therefore, replicates the typical nonlinear saturation mechanisms found in free-surface hydrodynamic oscillators near resonance conditions. The bifurcation structure also shows that the main nonlinear dynamics are driven by only a few interacting modes close to the onset of instability. Although the original hydrodynamic formulation comes from coupled free-surface partial differential equations, the Galerkin reduction effectively captures the transition to oscillatory instability using just a few nonlinear degrees of freedom. This confirms that the main hydrodynamic energy-transfer mechanisms are concentrated in the retained modal interactions, validating the reduced-order framework for continuation analysis and control studies.

The optimal-control results further emphasize the strong link between nonlinear hydrodynamic stability and wave-energy harvesting performance. The objective function aimed to maximize the power extracted through the power take-off mechanism while including a soft stability penalty related to the Hopf bifurcation structure. Comparing the uncontrolled and constrained optimization results shows that the stability-aware formulation leads to better energy-harvesting performance. When no stability measures were applied, the achieved objective value was 3.454. After adding the soft stability penalty formulation, the objective value rose to 3.79. This improvement suggests that steering the system away from Hopf-induced oscillatory instability allows the controller to work within a more favorable hydrodynamic environment for continuous energy extraction.

This result implies that excessive nonlinear oscillations near the instability boundary do not necessarily reflect optimal harvesting conditions. While resonance amplification can increase oscillation amplitudes, the related nonlinear limit-cycle dynamics may result in inefficient energy transfer, large transient responses, and increased hydrodynamic dissipation. By preventing strong self-excited oscillations, the stability-constrained controller keeps a better balance between wave forcing, hydrodynamic damping, and power extraction. The resulting dynamics thus allow for more efficient transfer of wave energy into the power take-off mechanism while avoiding destabilizing oscillatory growth. The rise in the objective value after implementing the stability penalty shows that bifurcation-aware control strategies can significantly impact wave-energy conversion efficiency. Rather than viewing bifurcation dynamics as solely negative, this formulation directly incorporates the underlying nonlinear stability structure into the optimization framework. This approach allows the controller to manage the system's proximity to instability while maximizing harvested power. Such a strategy is especially crucial for nonlinear ocean-energy systems, as efficient operating regimes often exist near resonance, where stability margins are tight. Figures 2a–2b and 2c–2d further display how the stability penalty affects the optimal control trajectories. Without the Hopf-related stabilization mechanism, the control profiles show stronger oscillatory variations near the system's approach to nonlinear instability. On the other hand, including the stability penalty produces smoother, more consistent control trajectories while increasing the energy-harvesting objective. This behavior indicates that the optimization process can discover operating conditions that enhance both energy performance and dynamic stability. The resulting controlled trajectories, therefore, correspond to hydrodynamically efficient operating states with less vulnerability to large-amplitude nonlinear oscillations.

Overall, the results demonstrate that the reduced-order nonlinear hydrodynamic oscillator effectively replicates the critical dynamical mechanisms governing nonlinear wave-structure interaction, including resonance amplification, nonlinear saturation, modal coupling, and Hopf bifurcation behavior. The continuation analysis confirms the onset of stable nonlinear oscillations through a supercritical Hopf bifurcation, while the optimal-control results illustrate that bifurcation-aware stabilization strategies can enhance energy-harvesting performance. The combined continuation and control framework thus offers a computationally manageable and physically consistent method for analyzing and optimizing nonlinear ocean-wave energy systems.

4. Conclusion

This study developed a reduced-order framework that considers bifurcation for analyzing and controlling the dynamics of nonlinear wave-energy converters using a coupled fluid-structure interaction model. Starting from a free-surface potential flow description of a floating point-absorber system, a Galerkin projection was used to create a low-dimensional nonlinear oscillator. This oscillator captures the essential hydrodynamic mechanisms that govern wave-buoy interaction. The resulting system reflects key physical processes, including resonance amplification, nonlinear restoring effects, radiation damping, and modal coupling through a secondary hydrodynamic interaction mode. Bifurcation analysis showed that the reduced-order system undergoes a supercritical Hopf bifurcation at the equilibrium state. This leads to the emergence of stable limit-cycle oscillations. The negative first Lyapunov coefficient confirms that the instability settles into bounded periodic motion rather than diverging dynamics.

This behavior aligns with nonlinear wave-structure interaction, where hydrodynamic nonlinearities control energy growth and lead to finite-amplitude oscillations suitable for energy harvesting. The presence of stable limit cycles highlights the importance of nonlinear effects in determining the operating conditions of wave energy systems, especially near resonance. An optimal control formulation was then introduced to examine energy harvesting performance under various stability assumptions. The power take-off system was modeled as an active control input, and the objective function aimed to maximize instantaneous power extraction while restricting excessive control effort. A soft stability constraint regulated the distance to the Hopf bifurcation boundary. The results showed that maintaining stability-aware control improves the overall objective value, indicating that reducing excessive nonlinear oscillations can boost net energy extraction efficiency. The comparison between uncontrolled and controlled cases demonstrates that bifurcation-aware control strategies are vital for system performance. Optimal operation requires balancing energy extraction with nonlinear stability constraints, rather than just amplifying resonance effects. The improved performance achieved through stability regulation emphasizes the need to incorporate the structure of dynamical systems into control design. Overall, the study creates a unified framework for reduced-order modeling, bifurcation analysis, and optimal control of nonlinear wave-energy systems. The results indicate that blending hydrodynamic physics with nonlinear dynamical systems theory offers a powerful approach for understanding, predicting, and optimizing energy harvesting in complex ocean environments.

Data Availability Statement

All data used is presented in the paper

Conflict of Interest

The author, Dr. Lakshmi N Sridhar, has no conflict of interest.

Author Contribution

L. N Sridhar is the sole author of this paper

Acknowledgement

Dr. Sridhar thanks Dr. Carlos Ramirez for encouraging him to write single-author papers.

Funding

No funding was obtained for this research

References

[1] Johannes Falnes, and Adi Kurniawan, *Ocean Waves and Oscillating Systems Linear Interactions Including Wave-Energy Extraction*, 2nd ed., Cambridge University Press, pp. 1-300, 2020. [Google Scholar] [Publisher Link]

[2] Umesh A. Korde, "Latching Control of Deep-Water Wave Energy Devices using an Active Reference," *Ocean Engineering*, vol. 29, no. 11, pp. 1343-1355, 2002. [CrossRef] [Google Scholar] [Publisher Link]

[3] Alain Clément et al., "Wave Energy in Europe: Current Status and Perspectives," *Renewable and Sustainable Energy Reviews*, vol. 6, no. 5, pp. 405-431, 2002. [CrossRef] [Google Scholar] [Publisher Link]

[4] Aurélien Babarit, and Alain H. Clément, "Optimal Latching Control of a Wave Energy Device in Regular and Irregular Waves," *Applied Ocean Research*, vol. 28, no. 2, pp. 77-91, 2006. [CrossRef] [Google Scholar] [Publisher Link]

[5] D.V. Evans, "A Theory for Wave-Power Absorption by Oscillating Bodies," *Journal of Fluid Mechanics*, vol. 77, no. 1, pp. 1-25, 1976. [CrossRef] [Google Scholar] [Publisher Link]

[6] Johannes Falnes, "A Review of Wave-Energy Extraction," *Marine Structures*, vol. 20, no. 4, pp. 185-201, 2007. [CrossRef] [Google Scholar] [Publisher Link]

[7] Jørgen Hals, Johannes Falnes, and Torgeir Moan "Constrained Optimal Control of a Heaving Buoy Wave-Energy Converter," *Journal of Offshore Mechanics and Arctic Engineering*, vol. 133, no. 1, 2011. [CrossRef] [Google Scholar] [Publisher Link]

[8] A. Babarit, "On the Park Effect in Arrays of Oscillating Wave Energy Converters," *Renewable Energy*, vol. 58, pp. 68-78, 2013. [CrossRef] [Google Scholar] [Publisher Link]

[9] Edo Abraham, and Eric C. Kerrigan, "Optimal Active Control and Optimization of a Wave Energy Converter," *IEEE Transactions on Sustainable Energy*, vol. 4, no. 2, pp. 324-332, 2013. [CrossRef] [Google Scholar] [Publisher Link]

[10] Thor I. Fossen, *Handbook of Marine Craft Hydrodynamics and Motion Control*, 2nd ed., Wiley, pp. 1-500, 2014. [Google Scholar] [Publisher Link]

[11] Francesco Fusco, and John V. Ringwood, "Hierarchical Robust Control of Oscillating Wave Energy Converters with Uncertain Dynamics," *IEEE Transactions on Sustainable Energy*, vol. 5, no. 3, pp. 958-966, 2014. [CrossRef] [Google Scholar] [Publisher Link]

[12] Shangyan Zou et al., "Optimal Control of Wave Energy Converters," *Renewable Energy*, vol. 103, pp. 217-225, 2017. [CrossRef] [Google Scholar] [Publisher Link]

[13] John V. Ringwood, Giorgio Bacelli, and Francesco Fusco, "Energy-Maximizing Control of Wave-Energy Converters: The Development of Control System Technology to Optimize Their Operation," *IEEE Control Systems Magazine*, vol. 34, no. 5, pp. 30-55, 2014. [CrossRef] [Google Scholar] [Publisher Link]

[14] J. Falnes, "Wave-Energy Conversion Through Relative Motion Between Two Single-Mode Oscillating Bodies," *Journal of Offshore Mechanics and Arctic Engineering*, vol. 121, no. 1, pp. 32-38, 1999. [CrossRef] [Google Scholar] [Publisher Link]

[15] Rudy Nie et al., "Optimal Causal Control of Wave Energy Converters in Stochastic Waves – Accommodating Nonlinear Dynamic and Loss Models," *International Journal of Marine Energy*, vol. 15, pp. 41-55, 2016. [CrossRef] [Google Scholar] [Publisher Link]

[16] Shangyan Zou et al., "Optimal Control of Wave Energy Converters," *Renewable Energy*, vol. 103, pp. 217-255, 2017. [CrossRef] [Google Scholar] [Publisher Link]

[17] Giorgio Bacelli, Romain Genest, and John V. Ringwood, "Nonlinear Control of Flap-Type Wave Energy Converter with a Non-Ideal Power Take-Off System☆," *Annual Reviews in Control*, vol. 40, pp. 116-126, 2015. [CrossRef] [Google Scholar] [Publisher Link]

[18] Alexis Mérigaud, and John V. Ringwood, "A Nonlinear Frequency-Domain Approach for Numerical Simulation of Wave Energy Converters," *IEEE Transactions on Sustainable Energy*, vol. 9, no. 1, pp. 86 - 94, 2018. [CrossRef] [Google Scholar] [Publisher Link]
[19] Aleix Maria-Arenas et al., "Control Strategies Applied to Wave Energy Converters: State of the Art," *Energies*, vol. 12, no. 16, pp. 1-19, 2019. [CrossRef] [Google Scholar] [Publisher Link]
[20] Kshitij Mall, and Ehsan Taheri, "Optimal Control of Wave Energy Converters using Epsilon-Trig Regularization," *arXiv preprint*, pp. 1-6, 2019. [CrossRef] [Google Scholar] [Publisher Link]
[21] Luca Parrinello et al., "An Adaptive and Energy-Maximizing Control Optimization of Wave Energy Converters using an Extremum-Seeking Approach," *Physics of Fluids*, vol. 32, no. 11, 2020. [CrossRef] [Google Scholar] [Publisher Link]
[22] LiGuo Wang et al., "Improving Electric Power Generation of a Standalone Wave Energy Converter Via Optimal Electric Load Control," *arXiv preprint*, pp. 1-11, 2020. [CrossRef] [Google Scholar] [Publisher Link]
[23] Mertcan Yetkin et al., "Practical Optimal Control of a Wave-Energy Converter in Regular Wave Environments," *arXiv preprint*, pp. 1-24, 2021. [CrossRef] [Google Scholar] [Publisher Link]
[24] Thor I. Fossen. "A Nonlinear Unified State-Space Model for Ship Maneuvering and Control in a Seaway," *International Journal of Bifurcation and Chaos*, vol. 15, no. 9, pp. 2717-2746, 2023. [CrossRef] [Google Scholar] [Publisher Link]
[25] A. Dhooge, W. Govaerts, and Yu. A. Kuznetsov, "MATCONT: A MATLAB Package for Numerical Bifurcation Analysis of ODEs," *ACM transactions on Mathematical Software*, vol. 29, no. 2, pp. 141-164, 2003. [CrossRef] [Google Scholar] [Publisher Link]
[26] Yuri A. Kuznetsov, *Elements of Applied Bifurcation Theory*, 2nd ed., Springer, NY, 1998. [CrossRef] [Google Scholar] [Publisher Link]
[27] Willy J.F. Govaerts, "Numerical Methods for Bifurcations of Dynamical Equilibria," *SIAM*, 2000. [Google Scholar]
[28] Andreas Wächter, and Lorenz T. Biegler, "On the Implementation of an Interior-Point Filter Line-Search Algorithm for Large-Scale Nonlinear Programming," *Mathematical Programming*, vol. 106, no. 1, pp. 25-57, 2006. [CrossRef] [Google Scholar] [Publisher Link]

Appendix

In this appendix, all the formulae for the various parameters are derived.

Derivation for ω^2

$$\int_\Omega R_\eta \, \Phi_1 \, d\Omega = 0$$

$$\int_\Omega (g\eta + \nabla\phi \cdot \nabla\phi) \, \Phi_1 \, d\Omega = 0$$

$$\omega^2 x = \int_\Omega \Phi_1 \, (g\Phi_1 x + \nabla\Phi_1 \cdot \nabla\Phi_1 x) d\Omega$$

$$\omega^2 = \int_\Omega \Phi_1 \, (g\Phi_1 + \nabla\Phi_1 \cdot \nabla\Phi_1) d\Omega$$

Derivation for μ

$$\int_\Omega R_\phi \, \Psi_1 \, d\Omega = 0$$

$$\int_\Omega \frac{\partial\phi}{\partial t} \Psi_1 \, d\Omega = 0$$

$$\mu y = \int_\Omega \Phi_1 \frac{\partial\Phi_1}{\partial t} y \, d\Omega$$

$$\mu = \int_\Omega \Phi_1 \frac{\partial\Phi_1}{\partial t} \, d\Omega$$

Derivation for α

$$\int_\Omega R_\eta \, \Phi_1 \, d\Omega = 0$$

$$\int_\Omega (\eta^3 + \eta_b \eta^2) \, \Phi_1 \, d\Omega = 0$$

$$\alpha x^3 = \int_\Omega \Phi_1 \, (\Phi_1^3 x^3 + \eta_b \Phi_1^2 x^2) d\Omega$$

$$\alpha = \int_\Omega \Phi_1 \, (\Phi_1^3 + \eta_b \Phi_1^2) d\Omega$$

Derivation for β

$$\int_\Omega R_\phi \, \Psi_1 \, d\Omega = 0$$
$$\int_\Omega \left(\eta^2 \frac{\partial \phi}{\partial t} + \nabla\phi \cdot \nabla \frac{\partial \phi}{\partial t}\right) \Psi_1 \, d\Omega = 0$$
$$\beta x^2 y = \int_\Omega \Phi_1 \left(\Phi_1^2 x^2 y + \nabla\Phi_1 \cdot \nabla \frac{\partial \Phi_1}{\partial t} x^2 y\right) d\Omega$$
$$\beta = \int_\Omega \Phi_1 \left(\Phi_1^2 \frac{\partial \Phi_1}{\partial t} + \nabla\Phi_1 \cdot \nabla \frac{\partial \Phi_1}{\partial t}\right) d\Omega$$

Derivation for γ

$$\int_\Omega R_\phi \, \Psi_3 \, d\Omega = 0$$
$$\int_\Omega \left(\frac{\partial \Psi_3}{\partial t} + g\Psi_3 + \nabla\Phi_1 \cdot \nabla\Psi_3\right) \Phi_1 \, d\Omega = 0$$
$$\gamma z = \int_\Omega \Phi_1 \left(\frac{\partial \Psi_3}{\partial t} z + g\Psi_3 z\right) d\Omega + \int_\Omega \Phi_1 \, \nabla\Phi_1 \cdot \nabla\Psi_3 z \, d\Omega$$
$$\gamma = \int_\Omega \Phi_1 \left(\frac{\partial \Psi_3}{\partial t} + g\Psi_3\right) d\Omega + \int_\Omega \Phi_1 \, \nabla\Phi_1 \cdot \nabla\Psi_3 \, d\Omega$$

Derivation for λ

$$\int_\Omega R_\phi \, \Psi_3 \, d\Omega = 0$$
$$\int_\Omega \left(\frac{\partial \Psi_3}{\partial t} + \nabla\Psi_3 \cdot \nabla\Psi_3\right) \Psi_3 \, d\Omega = 0$$
$$\lambda z = \int_\Omega \Psi_3 \left(\frac{\partial \Psi_3}{\partial t} z + \nabla\Psi_3 \cdot \nabla\Psi_3 z\right) d\Omega$$
$$\lambda = \int_\Omega \Psi_3 \left(\frac{\partial \Psi_3}{\partial t} + \nabla\Psi_3 \cdot \nabla\Psi_3\right) d\Omega$$

Derivation for δ

$$\int_\Omega R_\eta \, \Psi_3 \, d\Omega = 0$$
$$\int_\Omega (\eta^2 + \nabla\phi \cdot \nabla\phi) \, \Psi_3 \, d\Omega = 0$$
$$\delta x^2 = \int_\Omega \Psi_3 \, (\Phi_1^2 x^2 + \nabla\Phi_1 \cdot \nabla\Phi_1 x^2) d\Omega$$
$$\delta = \int_\Omega \Psi_3 \, (\Phi_1^2 + \nabla\Phi_1 \cdot \nabla\Phi_1) d\Omega$$

Derivation for σ

$$\int_\Omega R_\phi \, \Psi_3 \, d\Omega = 0$$
$$\int_\Omega \left(\eta \frac{\partial \phi}{\partial t} + \nabla\phi \cdot \nabla \frac{\partial \phi}{\partial t}\right) \Psi_3 \, d\Omega = 0$$
$$\sigma xy = \int_\Omega \Psi_3 \left(\Phi_1 xy \frac{\partial \Phi_1}{\partial t} + \nabla\Phi_1 \cdot \nabla \frac{\partial \Phi_1}{\partial t} xy\right) d\Omega$$
$$\sigma = \int_\Omega \Psi_3 \left(\Phi_1 \frac{\partial \Phi_1}{\partial t} + \nabla\Phi_1 \cdot \nabla \frac{\partial \Phi_1}{\partial t}\right) d\Omega$$

Table 1. Summary of Variables in PDE

Variable	Meaning
(ϕ (x,y,z,t))	Velocity potential
(η (x,y,t))	Free-surface elevation
(η_b (t))	Vertical buoy displacement
you	Fluid velocity vector
(p)	Fluid pressure
F_h	Hydrodynamic force
F_w	Incident wave forcing
u(t)	Control input associated with the power take-off system
g	Gravitational acceleration
h	Water depth
t	Time

Table 2. Summary of Parameters in PDE

Parameter	Meaning
(m)	Buoy mass
m_a	Hydrodynamic added mass
c_r	Radiation damping coefficient
c_{PTO}	Power take-off damping coefficient
k_h	Hydrostatic restoring stiffness
α	Cubic nonlinear stiffness coefficient
β	Nonlinear damping coefficient
ρ	Fluid density

Table 3. Variables (3-ODE Reduced System)

Variable	Meaning
(x(t))	Principal oscillatory wave–buoy mode (dominant displacement mode)
(y(t))	Velocity of the principal oscillatory mode (dx/dt)
(z(t))	Secondary hydrodynamic interaction mode (fluid memory/radiation effects)
(t)	Time

Table 4. Parameters (3-ODE Reduced System)

Parameter	Meaning
ω	Natural frequency of the wave–buoy oscillatory mode
μ	Effective linear hydrodynamic damping/growth rate
α	Cubic nonlinear stiffness coefficient (saturation nonlinearity)
β	Nonlinear damping coefficient (amplitude-dependent dissipation)
γ	Coupling strength between primary mode $x$and hydrodynamic mode z
λ	Relaxation rate of secondary hydrodynamic mode
δ	Quadratic forcing coefficient generating z-mode from x^2
σ	Mixed nonlinear interaction coefficient between $x$and y

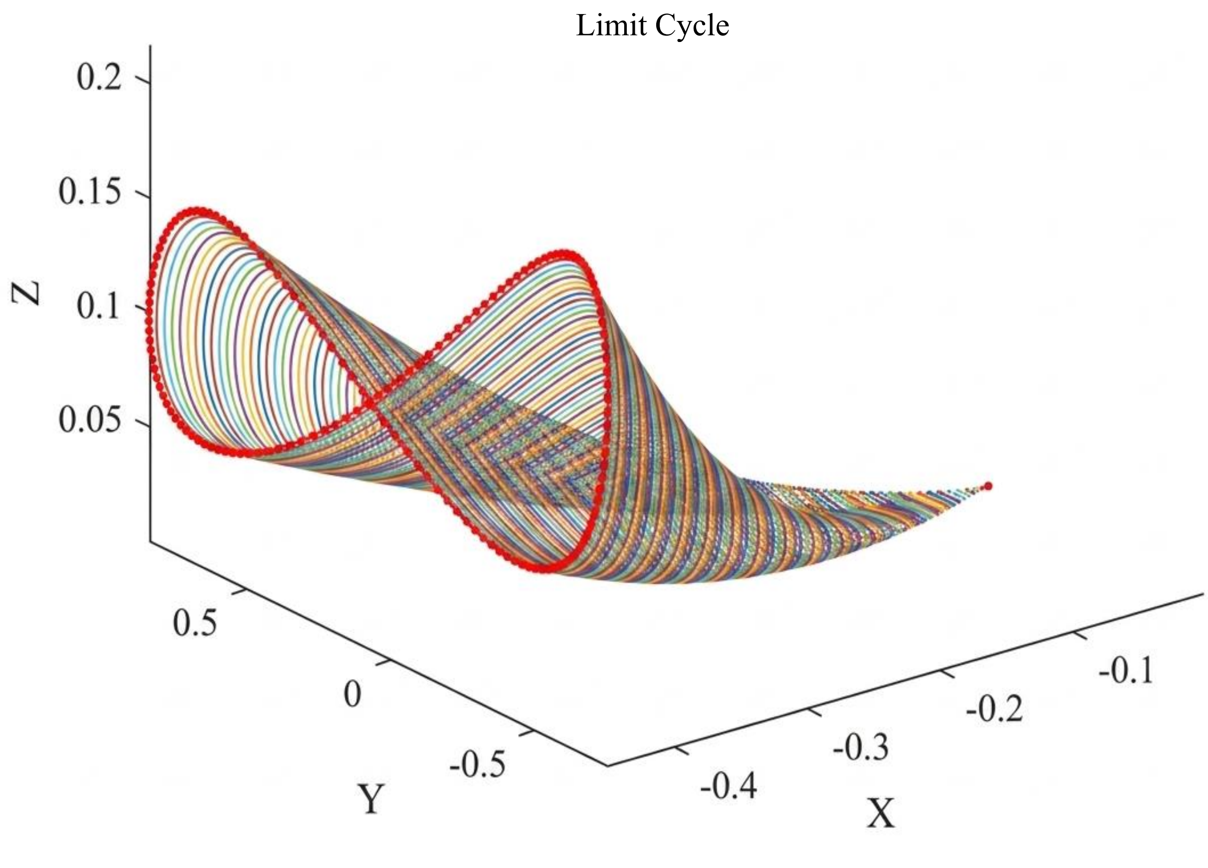

Fig. 1(a) Limit Cycle caused by Hopf Bifurcation

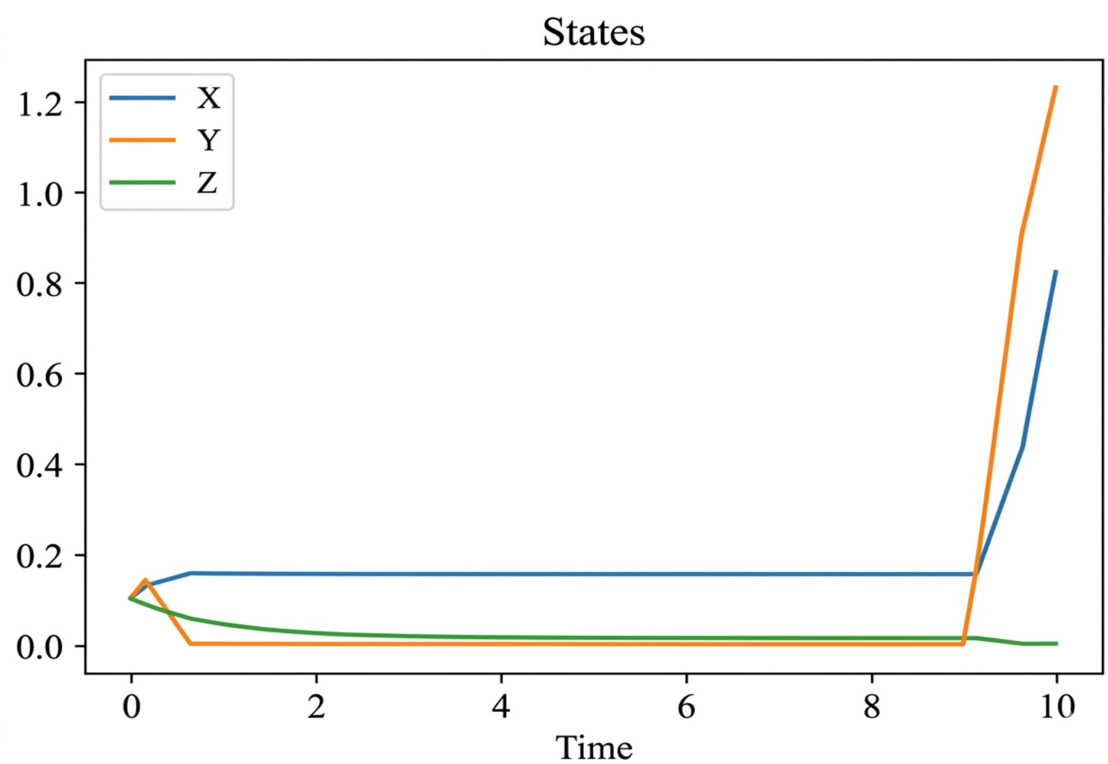

Fig. 2(a) Optimal Control X, Y, Z, No Hopf constraint

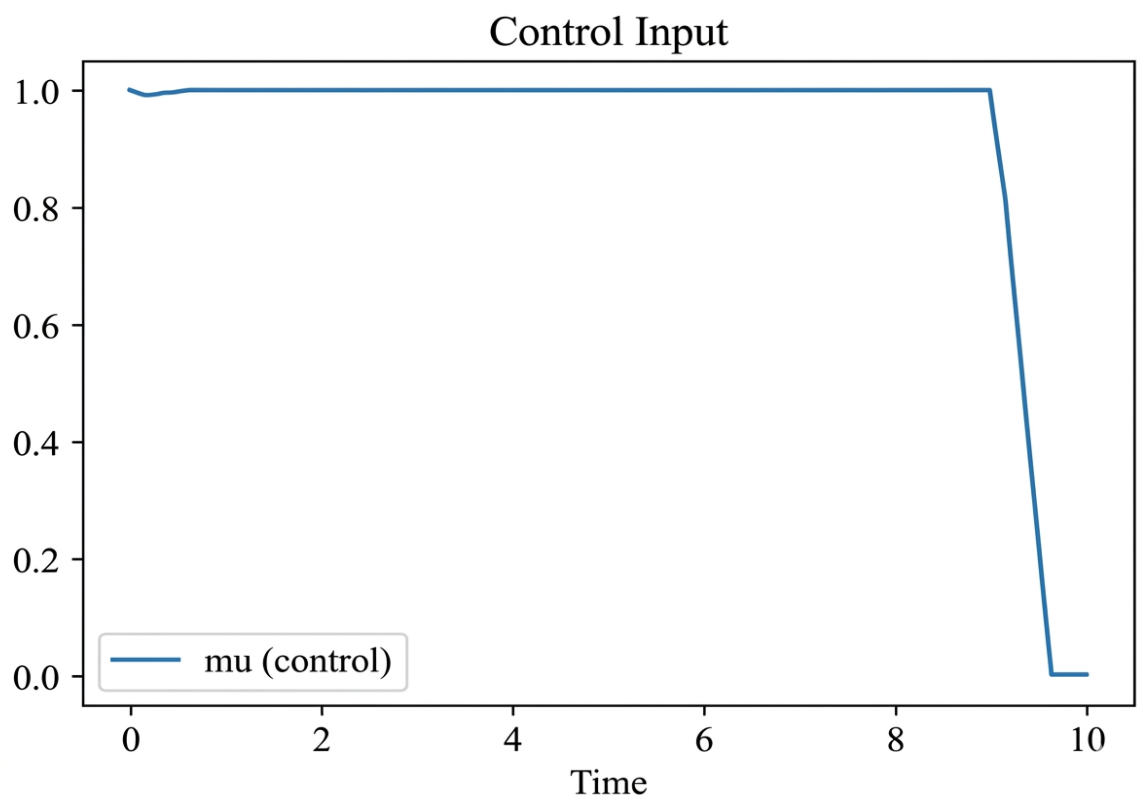

Fig. 2(b) Optimal Control μ No Hopf constraint

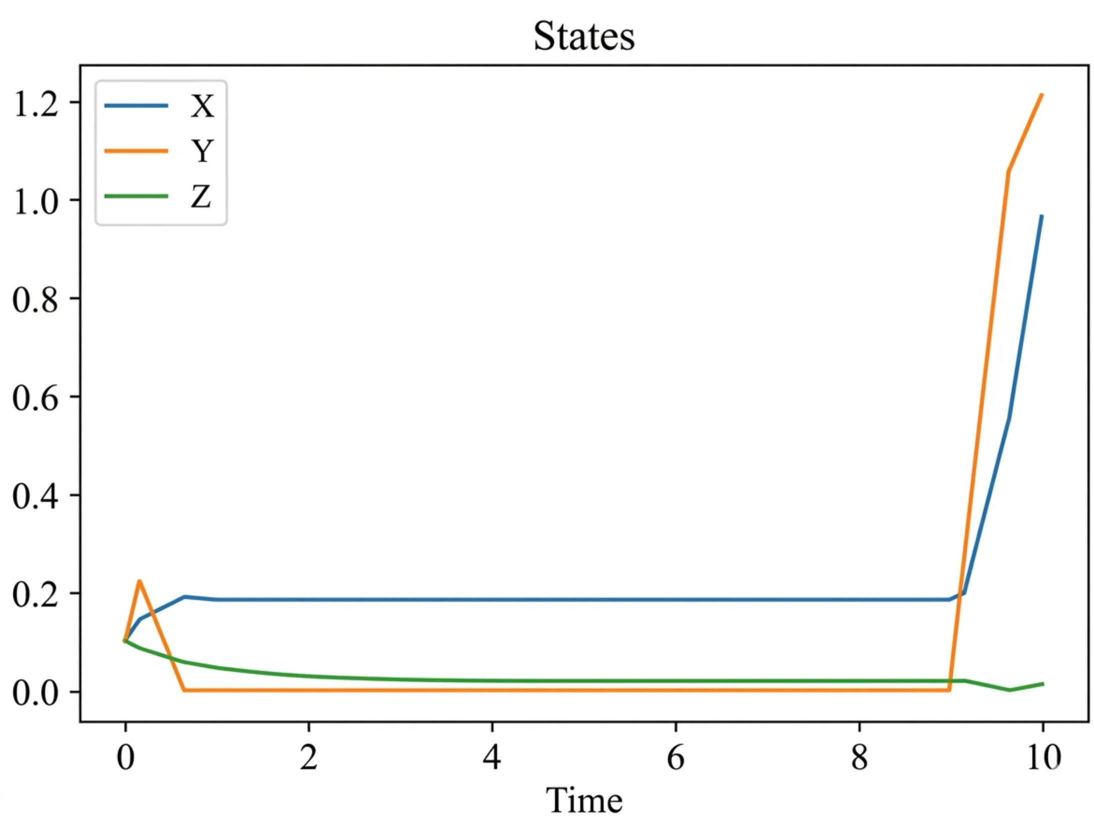

Fig. 2(c) Optimal Control X, Y, Z, with Hopf constraint

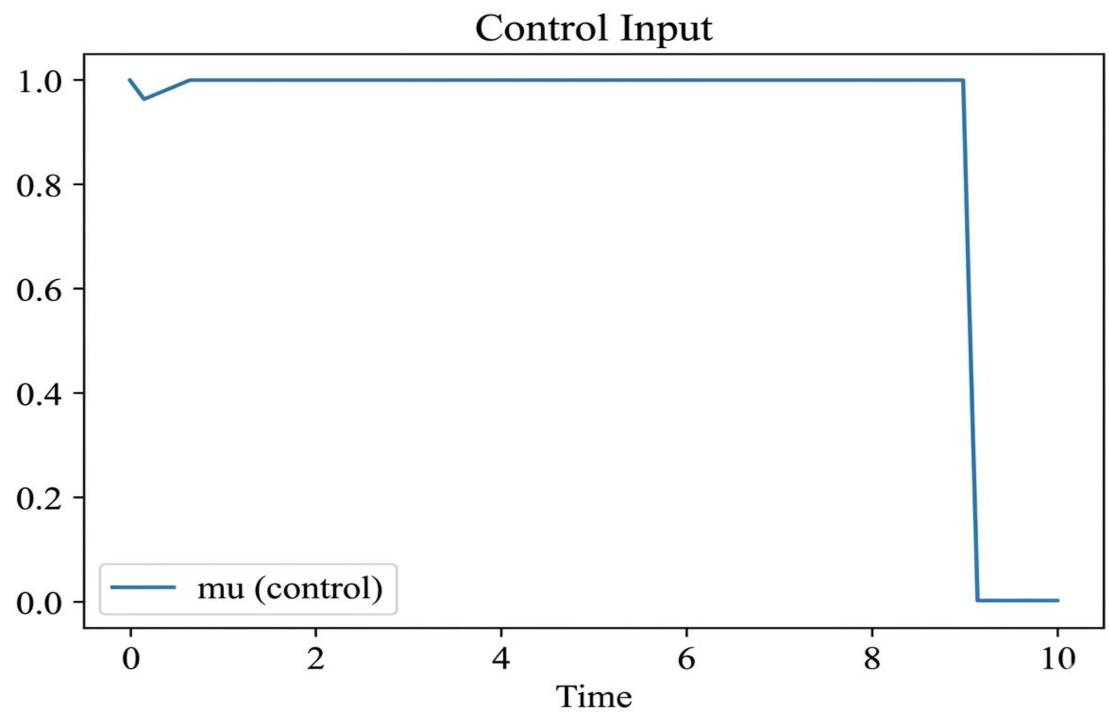

Fig. 2(d) Optimal Control μ with Hopf constraint